Structure and Magnetic Ordering of $M^{II}[N(CN)_2]_2$ (M = Co, Ni)†

Jamie L. Manson,[1a] Carmen R. Kmety,[1b] Qing-zhen Huang,[1c] Jeffrey W. Lynn,[1c] Goetz M. Bendele,[1d] Silvina Pagola,[1d] Peter W. Stephens,[1d] Louise M. Liable-Sands,[1e] Arnold L. Rheingold,[1e] Arthur J. Epstein,*[,1b] and Joel S. Miller*[,1a]

Department of Chemistry, University of Utah, Salt Lake City, Utah 84112-0850, Department of Physics and the Department of Chemistry, The Ohio State University, Columbus, Ohio 43210-1106, NIST Center for Neutron Research, National Institute of Standards and Technology, Gaithersburg, Maryland 20899, the Department of Physics and Astronomy, State University of New York, Stony Brook, New York 11794-3800, and the National Synchrotron Light Source, Brookhaven National Laboratory, Upton, New York 11973

Received May 1, 1998. Revised Manuscript Received June 30, 1998

The reaction of $[M^{II}(OH_2)_6](NO_3)_2$ (M = Co, Ni) and $[N(CN)_2]^-$ leads to formation of isomorphous $M[N(CN)_2]_2$ [M = Co (**2a**), Ni (**3**)], respectively, while the reaction of $[Co^{II}(OH_2)_6](NO_3)_2$ in 1% pyridine (py) solution with $[N(CN)_2]^-$ leads to the formation of $Co[N(CN)_2]_2py_2$. The structure of **2a**, α-$Co[N(CN)_2]_2$, was determined from the Rietveld analyses of both powder X-ray (synchrotron) and neutron as well as single-crystal X-ray diffraction data, whereas the structure of **3** was determined from the Rietveld analysis of powder neutron diffraction data. **2a** (pink) and **3** (light blue) belong to the orthorhombic space group *Pnnm* with $Z = 2$ [**2a** (single crystal): $a = 5.9985(15)$, $b = 7.0711(18)$, $c = 7.4140(19)$ Å, $V = 314.47(14)$ Å^3, $R_1 = 0.027$. **3** (powder neutron diffraction): $a = 5.97357(25)$, $b = 7.03196(28)$, $c = 7.29424(22)$ Å, $V = 306.40(3)$ Å^3, $\chi^2 = 1.650$]. Thermolysis of $Co[N(CN)_2]_2py_2$ leads to intensely blue β-$Co^{II}[N(CN)_2]_2$, **2b**. The M in **2a** and **3** are six-coordinate and bound to six different μ_3-bonded $[N(CN)_2]^-$ ligands, forming a rutile-like 3-D framework. Both M^{II} sites are slightly tetragonally elongated, with average axial M−N distances (295 K) of 2.161(5) (**2a**) and 2.137(2) Å (**3**) and average equatorial M−N distances of 2.091(4) (**2a**) and 2.051(1) Å (**3**), and each M^{II} is coordinated to four equatorial $[N(CN)_2]^-$ ligands that bridge between two adjacent M^{II} sites, generating ribbon-like 1-D chains that propagate along the *c*-axis. Adjacent chains pack out-of-registry, with the central N2s bridging to M^{II} ions of adjacent chains, forming a 3-D network. $[N(CN)_2]^-$ has pseudo-C_{2v} symmetry with average C1≡N1 distances of 1.158 (**2a**) and 1.159 Å (**3**) at room temperature and C1−N2 distances of 1.315 (**2a**) and 1.313 Å (**3**). The structure of **2b** has not yet been elucidated, but on the basis of the color and magnetic properties, it is thought to be comprised of tetrahedral Co(II). The shortest M···M separations are 5.936 (**2a**) and 5.881 Å (**3**) at room temperature via neutron diffraction studies. The susceptibility for **2a**, **2b**, and **3** can be fit by the Curie−Weiss expression with $g = 2.60$, $\theta = 9$ K ($T > 50$ K); $g = 2.27$, $\theta = -7$ K ($T > 60$ K); and $g = 2.20$, $\theta = 21$ K ($T > 50$ K), respectively. The observed room-temperature effective moments of 5.13, 4.37, and 3.17 μ_B, respectively, exceed the spin-only moments as expected for these metal ions, but are consistent with octahedral Co(II), tetrahedral Co(II), and octahedral Ni(II), respectively. Ferromagnetic behavior is suggested for **2a** and **3** from the 5 K, 5.5 T saturation magnetizations of 14 000 (**2a**) and 11 900 emu Oe/mol (**3**), hysteresis loops with coercive fields, H_{cr}, of 800 (**2a**), 680 (**2b**), and 7000 Oe (**3**) at 2 K, field-cooled and zero-field-cooled low-field $M(T)$ data showing magnetic ordering below essentially magnetic field-independent bifurcation temperatures of 9.2 (**2a**) and 20.6 K (**3**), and observations of both in-phase, $\chi'(T)$, and out-of-phase, $\chi''(T)$, components of the ac susceptibility maxima slightly below the bifurcation temperatures. The T_cs are estimated from the peaks in the 10 Hz $\chi'(T)$ data to be 8.7, 8.9, and 19.7 K for **2a**, **2b**, and **3**, respectively. Using mean-field theory the spin-coupling energies, J/k_B, were estimated to be 0.45, −0.7, and 2.0 K for **2a**, **2b**, and **3**, respectively. **2b** shows canted antiferromagnetic behavior below its ordering temperature of 8.9 K. A second transition at 2.7 K, as observed in ac susceptibility, specific heat, and field-cooled/zero-field-cooled magnetization studies, suggests the possibility of an initially canted antiferromagnetic ground state with a change in canting angle below 2.7 K.

Introduction

The quest to develop new magnets based on molecular precursors is a growing area of contemporary materials chemistry research.[2,3] Molecule-based magnets today span materials with spins solely residing in p-orbitals, e.g., a few nitroxides,[4] to materials with spins solelyresiding in d-orbitals, e.g., mixed-metal hexacyanides[5] and

† This paper is dedicated to the memory of Jean Rouxel.

S0897-4756(98)00321-4 CCC: $15.00
Published on Web 08/27/1998

tris(oxalato)[6] complexes, with several examples of materials with spins residing in both p- and d-orbitals that are either not connected via covalent bonding, e.g., $[FeCp^*_2]^{\bullet+}[TCNE]^{\bullet-}$,[3c] or are connected via covalent bonding, e.g., $Mn(hfac)_2$(nitroxide),[3c,7] [Mn(porphyrin)][TCNE],[3c,8] and $M(TCNE)_2$ (M = V, Mn, Fe, Co, Ni).[3c,9] Magnetic ordering temperatures, T_c, range from 400 K (125 °C) for the latter $V(TCNE)_2$ magnet[1c,9] to below 1.5 K for the nitroxides,[4b] albeit some organic weak/canted magnets have T_c values as high as 35.5 K, but possess only 0.15% of the expected magnetization.[10]

Spin-bearing metal ions linked via six cyanide ligands have enabled the development of several 3-D structured ferro- or ferrimagnets ordering with T_cs as high as 315 K,[5] depending on the metal ions. In addition to extending this to four-coordinate systems,[11a] other nitrile-containing bridging ligands are being studied.[11b] Due to the potential of being polydentate, we have investigated the homoleptic coordination chemistry of dicyanamide, $[N(CN)_2]^-$. $[N(CN)_2]^-$ can act as a terminal ligand (**1a**), as observed for $[Cu^{II}(o\text{-phen})_2(N(CN)_2][C(CN)_3]$[12a] and $[Cu^{II}(o\text{-phen})_2[N(CN)_2]_2]$[12b] (*o*-phen = *o*-phenanthrolene), or as a μ- (**1b,c**), μ_3- (**1d**), or μ_4- (**1e**) bridging ligand. **1b** was reported for $Me_2Sn[(N(CN)_2]_2$,[12c] $Me_3Sn(N(CN)_2$,[12c] and $Ag[N(CN)_2]$,[12d] and **1e** was observed for $Me_2Tl[N(CN)_2]$.[12e] Linkage isomerization between **1b** and **1c** has been postulated for $Cu^{II}[N(CN)_2]$-$(imidazole)_2$ with spin coupling via **1b** and **1c** resulting in antiferromagnetic and ferromagnetic coupling, respectively.[12f] **1d** was proposed for α-$M^{II}[N(CN)_2]_2$ (M = Mn, Fe, Co, Ni, Cu) on the basis of vibrational and electronic spectroscopy.[13] Herein, the structure and detailed magnetic properties of $M^{II}[N(CN)_2]_2$ [M = Co (**2**), Ni (**3**)] are described. A preliminary report on the magnetic properties of $M^{II}[N(CN)_2]_2$ [M = Co (**2**), Ni (**3**), and Cu] as well as the structure for M = Cu has appeared while we were writing this full paper.[14]

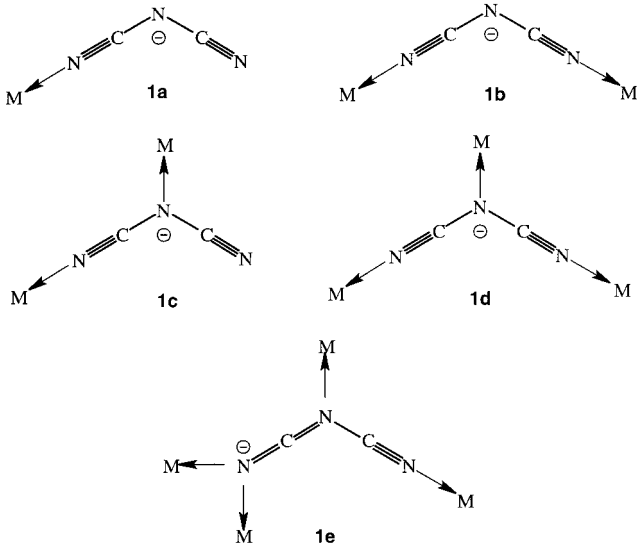

Experimental Section

$Na[N(CN)_2]_2$ (Aldrich), $[Co^{II}(OH_2)_6](NO_3)_2$ (Merck), and $[Ni^{II}(OH_2)_6](NO_3)_2$ (Baker) were used as purchased. $M^{II}[N(CN)_2]_2$ was synthesized by a route similar to that previously reported.[13]

(1) (a) University of Utah. (b) The Ohio State University. (c) NIST. (d) SUNY Stony Brook. (e) University of Delaware.

(2) *Proceedings on the Conference on Ferromagnetic and High Spin Molecular Based Materials*; Miller, J. S., Dougherty, D. A., Eds.; *Mol. Cryst., Liq. Cryst.* **1989**, *176. Proceedings on the Conference on Molecular Magnetic Materials*; Kahn, O., Gatteschi, D., Miller, J. S., Palacio, F., Eds; *NATO ARW Molecular Magn. Mater.* **1991**, *E198. Proceedings on the Conference on the Chemistry and Physics of Molecular Based Magnetic Materials*; Iwamura, H., Miller, J. S., Eds.; *Mol. Cryst., Liq. Cryst.* **1993**, *232/233. Proceedings on the Conference on Molecule-based Magnets*; Miller, J. S., Epstein, A. J., Eds.; *Mol. Cryst., Liq. Cryst.* **1995**, *271−274. Proceedings on the Conference on Molecular-Based Magnets*; Itoh, K., Miller, J. S., Takui, T., Eds.; *Mol. Cryst., Liq. Cryst.* **1997**, *305/306*. Turnbull, M. M.; Sugimoto, T.; Thompson, L. K. (Eds.) *Am. Chem. Soc. Symp. Ser.* **1996**, *644*.

(3) Reviews: (a) Buchachenko, A. L. *Russ. Chem. Rev.* **1990**, *59*, 307. *Usp. Khim.* **1990**, *59*, 529. Kahn, O. *Struct. Bonding* **1987**, *68*, 89. Kahn, O. *Molecular Magnetism*; VCH Publishers: New York, 1993. (b) Caneschi, A.; Gatteschi, D.; Sessoli, R.; Rey, P. *Acc. Chem. Res.* **1989**, *22*, 392. Gatteschi, D. *Adv. Mater.* **1994**, *6*, 635. (c) Miller, J. S.; Epstein, A. J.; Reiff, W. M. *Acc. Chem. Res.* **1988**, *21*, 114. Miller, J. S.; Epstein, A. J.; Reiff, W. M. *Science* **1988**, *240*, 40. Miller, J. S.; Epstein, A. J.; Reiff, W. M. *Chem. Rev.* **1988**, *88*, 201. Miller, J. S.; Epstein, A. J. *New Aspects of Organic Chemistry;* Yoshida, Z., Shiba, T., Ohsiro, Y., Eds.; VCH Publishers: New York, 1989; Vol. 237. Miller, J. S.; Epstein, A. J. *Angew. Chem., Int. Ed. Engl.* **1994**, *33*, 3, 385; *Angew. Chem.* **1994**, *106*, 399. Miller, J. S.; Epstein, A. J. *Adv. Chem. Ser.* **1995**, *245*, 161.

(4) (a) Kinoshita, M. *Jpn. J. Appl. Phys.* **1994**, *33*, 5718. (b) Chiarelli, R.; Rassat, A.; Dromzee, Y.; Jeannin, Y.; Novak, M. A.; Tholence, J. L. *Phys. Scrip.* **1993**, *T49*, 706.

(5) (a) Gadet, V.; Mallah, T.; Castro, I.; Verdaguer, M. *J. Am. Chem. Soc.* **1992**, *114*, 9213. (b) Mallah, T.; Ferlay, S.; Auberger, C.; Helary, C.; L′Hermite, F. Ouahes, F.; Vaissermann, J.; Verdaguer, M.; Veillet, P. *Mol. Cryst., Liq. Cryst.* **1995**, *273*, 141. (c) Ferlay, S.; Mallah, T.; Ouahes, R.; Veillet, P.; Verdaguer, M. *Nature* **1995**, *378*, 701. (d) Entley, W. R.; Girolami, G. S. *Science* **1995**, *268*, 397. (e) Entley, W. R.; Girolami, G. S. *Inorg. Chem.* **1994**, *33*, 5165. (f) Entley, W. R.; Treadway, C. R.; Girolami, G. S. *Mol. Cryst., Liq. Cryst.* **1995**, *273*, 153.

(6) For example: Tamaki, H.; Zhong, Z. J.; Matsumoto, N.; Kida, S.; Koikawa, K.; Achiwa, N.; Okawa, H. *J. Am. Chem. Soc.* **1992**, *114*, 6974. Mathoniere, C.; Nuttall, C. J.; Carling, S. G.; Day, P. *Inorg. Chem.* **1996**, *35*, 1201. Decurtins, S.; Schmalle, H. W.; Schneuwly, P.; Ensling, J.; Gütlich, P. *J. Am. Chem. Soc.* **1994**, *116*, 9521.

(7) Iwamura, H.; Inoue, K.; Hayamizu, T. *Pure App. Chem.* **1996**, *68*, 243. Gatteschi, D. *Adv. Mater.* **1994**, *6*, 635. Caneschi, A.; Gatteschi, D.; Sessoli R.; Rey, P. *Acc. Chem. Res.* **1989**, *22*, 392. Caneschi A.; Gatteschi, D.; Rey, P *Progr. Inorg. Chem.* **1991**, *37*, 331.

(8) Miller, J. S.; Epstein, A. J. *J. Chem. Soc., Chem. Commun.* **1998**, 1319.

(9) (a) Manriquez, J. M.; Yee, G. T.; McLean, R. S.; Epstein, A. J.; Miller, J. S. *Science* **1991**, *252*, 1415. Miller, J. S.; Yee, G. T.; Manriquez, J. M.; Epstein, A. J. In *The Proceedings of Nobel Symposium #NS-81 Conjugated Polymers and Related Materials: The Interconnection of Chemical and Electronic Structure*; Oxford University Press: 1993; p 461. *La Chim., La Ind.* **1992**, *74*, 845. Epstein, A. J.; Miller, J. S. In *The Proceedings of Nobel Symposium #NS-81 Conjugated Polymers and Related Materials: The Interconnection of Chemical and Electronic Structure*, Oxford University Press: 1993; p 475. *La Chim., La Ind.* **1993**, *75*, 185. Zhang, J.; Zhou, P.; Brinckerhoff, W. B.; Epstein, A. J.; Vazquez, C.; McLean, R. S.; Miller, J. S. *Am. Chem. Soc. Symp. Ser.* **1996**, *644*, 311.

(10) Banister, A. J.; Brickelbank, N.; Lavender, I.; Rawson, J. M.; Gregory, Tanner, B. K.; Clegg, W.; Elsegood, M. R. J.; Palacio, F. *Angew. Chem., Int. Ed. Engl.* **1996**, *35*, 2533. Palacio, F.; Antorrena, G.; Castro, M.; Burrriel, R.; Rawson, J.; Smith, N.; Brickelbank, N.; Novoa, J.; Ritter, C. *Phys. Rev. Lett.* **1997**, *79*, 2336.

(11) (a) Manson, J. L.; Buschmann, W. E.; Miller, J. S. *Angew. Chem., Int. Ed. Engl.* **1998**, *37*, 783. (b) Manson, J. L.; Campana, C.; Miller, J. S. *J. Chem. Soc., Chem. Commun.* **1998**, 151. (c) Manson, J. L.; Ressouche, E.; Miller, J. S. Manuscript in preparation.

(12) (a) Potocnak, I.; Dunaj-Jurco, M.; Miklos, D.; Jager, J. *Acta Crystallogr.* **1996**, *C52*, 1653. (b) Potocnak, I.; Dunaj-Jurco, M.; Miklos, D.; Kabesova, M.; Jager, J. *Acta Crystallogr.* **1995**, *C51*, 600. (c) Chow, Y. M. *Inorg. Chem.* **1971**, *10*, 1938. (d) Britton, D.; Chow, Y. M. *Acta Crystallogr.* **1977**, *B33*, 607. Britton, D. *Acta Crystallogr.* **1990**, *B46*, 2297. (e) Chow, Y. M.; Britton, D. *Acta Crystallogr.* **1975**, *B31*, 1934. (f) Mrozinski, J.; Hvastijova, M.; Kohout, J. *Polyhed.* **1992**, *11*, 2867.

(13) Köhler, H.; Kolbe, A.; Lux, G. *Z. Anorg. Allg. Chem.* **1977**, *428*, 103.

(14) (a) Batten, S. R.; Jensen, P.; Moubaraki, B.; Murray, K. S.; Robson, R. J. *Chem. Soc., Chem. Commun.* **1998**, 439. (b) Our preliminary work as well as that of M. Kurmoo was presented at the NATO ARW on Supramolecular Engineering of Synthetic Metallic Materials: Conductors and Magnets, Jan.10−14, 1998, Sitges, Spain. (d) Note that the structure reported in ref 14a is refined in the *Pnnm* space group with their *a*, *b*, and *c* axes corresponding to our *c*, *a*, and *b* axes, respectively.

α-Co[N(CN)$_2$]$_2$, 2a. [Co(OH$_2$)$_6$](NO$_3$)$_2$ (4.2784 g, 0.0147 mol) was dissolved in 40 mL of H$_2$O and quickly added to a 20 mL aqueous solution of Na[N(CN)$_2$] (3.2820 g, 0.037 mol), affording a red solution. After a short time, a pink solid precipitated from solution and was collected via vacuum filtration and dried in vacuo over P$_2$O$_5$ overnight, yielding 2.5270 g (90%) of an insoluble pink powder. Infrared spectra (Nujol): $\upsilon_{C\equiv N}$ 2199 vs, 2271 vs, 2310 m (sh), 2383 w cm^{-1}.

Co[N(CN)$_2$]$_2$py$_2$. A 100:1 v/v H$_2$O/pyridine solution of [Co(OH$_2$)$_6$](NO$_3$)$_2$ (1.48 mmol, 0.3688 g) was quickly added to a 5 mL aqueous solution of Na[N(CN)$_2$] (2.96 mmol, 0.2686 g), to afford a pink precipitate. The solid was collected via vacuum filtration and dried in vacuo over P$_2$O$_5$ for 2 h, yielding a pale pink powder in quantitative yield. Infrared spectra (Nujol): $\upsilon_{C\equiv N}$ 2295 s, 2242 s, 2179 vs cm^{-1}. Thermogravimetric analysis shows a single sharp weight loss of 45.17% at ca. 160 °C, consistent with loss of 2 equiv of coordinated pyridine ligands (45.30% calcd)

***β*-Co[N(CN)$_2$]$_2$, 2b**. Co[N(CN)$_2$]$_2$py$_2$ was transferred to a 10 mL Schlenk flask and heated in vacuo to 175 °C in an oil bath for 3 h. The color of the solid gradually changed from pink to intensely blue once the temperature had stabilized at 175 °C. $\upsilon_{C\equiv N}$ (Nujol): 2367 m, 2289 s, 2273 s, 2187 vs cm^{-1}.

Ni[N(CN)$_2$]$_2$, 3. [Ni(OH$_2$)$_6$](NO$_3$)$_2$ (4.4311 g, 0.015 mol) was dissolved in 40 mL of H$_2$O and quickly added to a 20 mL aqueous solution of Na[N(CN)$_2$] (3.3911 g, 0.038 mol), affording a green solution. After a short time, a blue solid precipitated from solution and was collected via vacuum filtration and dried in vacuo over P$_2$O$_5$ overnight, yielding 2.4873 g (87%) of an insoluble blue powder. Infrared spectra (Nujol): $\upsilon_{C\equiv N}$ 2206 vs, 2279 vs, 2312 m (sh), 2384 w cm^{-1}.

Spectroscopic Measurements. Infrared spectra were obtained on a Bio-Rad FTS-40 Fourier transform spectrometer in the range 600−4000 cm^{-1} using Nujol mulls sandwiched between NaCl plates. Diffuse reflectance optical data were obtained on an Hitachi U-3000 spectrophotometer with an integrated sphere attachment in the 250−800 nm range. The sample was finely ground and placed in a sealed quartz cell with a 1-mm path length. Alumina was used as a reference standard. Data were collected using a scan rate of 300 nm/min using a slit width of 4.0 nm.

Magnetic Measurements. DC magnetization measurements in the range 2−300 K were carried out using either a Quantum Design 5 T SQUID MPMS-5XL [equipped with reciprocating sample operation (RSO) transport, enhanced low temperature thermometry, and a magnet reset] or 5.5 T MPMS-5S magnetometers. AC susceptibility measurements were carried out using the 5 T MPMS-5XL SQUID magnetometer in the range 2−14 K for Co[N(CN)$_2$]$_2$ and 2−30 K for Ni[N(CN)$_2$]$_2$. Oscillating fields, with H_{ac} = 1 Oe, of 10, 100, and 1000 Hz were used in conjunction while H_{dc} = 0 Oe. Hysteresis experiments (to 5 T) were performed at 2, 5, and 8 K (**2a**), 2 and 6 K (**2b**), and 2, 11, and 20 K (**3**) upon careful zero-field cooling (ZFC) from 298 K after degaussing the μ-metal shield in conjunction with a Hall probe to null any residual magnetic field.

Thermal Measurements. Thermogravimetric analysis was performed using a TA model 2050 thermogravimetric analyzer between 25 and 500 °C. Specific heat data were obtained using a Quantum Design Physical Property Measurement System (PPMS). Each data point corresponds to a single relaxation measurement, where the sample holder is heated at constant power for half the characteristic time constant of the calorimeter, followed by a cooling period.[15] The 1.5 ± 0.5% temperature rise during heating constitutes the uncertainty in temperature for each point. The heat-capacity values were extracted from the temperature response curves by fitting to the solution of a dual time-constant thermal model, thus minimizing thermal contact artifacts.[16] On the basis of gold and copper standards, the absolute accuracy of the specific heat is estimated to be ±2%. All samples were mounted on sample holders using a small amount of Apiezon N grease. To separate the contribution of the sample heat capacity from the addenda, the heat capacity of the sample holder with the grease was measured over the full temperature range prior to mounting each sample. The sample masses used were 2.1 (**2a**), 1.2 (**2b**), and 3.3 (**3**) ± 0.1 mg.

Table 1. Crystallographic Details[a] for α-Co^{II}[N(CN)$_2$]$_2$ (2a) and Ni^{II}[N(CN)$_2$]$_2$ (3)

chemical form.	C_4N_6Ni	C_4N_6Co	C_4N_6Co	C_4N_6Co
form. mass, Da	191.02	191.02	191.02	190.78
space group	*Pnnm* (No. 58)	*Pnnm* (No. 58)	*Pnnm* (No. 58)	*Pnnm* (No. 58)
a, Å	5.97357(25)	5.9985(15)	5.98531(16)	6.0109(3)
b, Å	7.03196(28)	7.0711(18)	7.10298(16)	7.0724(4)
c, Å	7.29424(22)	7.4140(19)	7.39384(7)	7.3936(4)
V, Å^3	306.40(3)	314.47(14)	314.338(13)	314.32(3)
Z	2	2	2	2
T, K	198	295	295	295
λ, Å	1.5401	0.71073	1.5401	0.73335(2)
ρ_{calcd}, g/cm^3	2.067	2.017	2.017	2.02
μ, cm^{-1}		26.54		
R_1[b]		0.0217		
wR^2[c]		0.0549		
R_p[d]	0.0227		0.0222	0.0618
R_{wp}[e]	0.0287		0.0273	0.0780
χ^2[f]	1.650		1.482	1.92

[a] Methods: neutron, powder X-ray, single crystal neutron, powder synchrotron (includes anisotropic strain broadening of the Bragg peaks), and powder (includes anisotropic strain broadening of the Bragg peaks). [b] $\Sigma(|F_o| - |F_c|)/\Sigma |F_o|$. [c] $\{\Sigma w[F_o^2 - F_c^2]^2/\Sigma w[F_o^2]^2\}^{1/2}$. [d] $R_p = \Sigma|I_{oi} - I_{ci}|/\Sigma|I_{oi}|$. [e] $R_{wp} = (\Sigma w_i|I_{oi} - I_{ci}|^2/\Sigma|I_{oi}|^2)^{1/2}$. [f] $\chi^2 = R_{wp}^2/R_{exp}^2$.

Diffraction Studies. *Synchrotron Powder X-ray Structure Determination*. The structure of pink α-[Co[N(CN)$_2$]$_2$ was determined from a powder sample using high-resolution synchrotron X-ray powder diffraction at room temperature, ca. 295 K. The sample, approximately 10 mg, was sealed in a standard glass capillary of 0.7 mm diameter, and powder diffraction data were collected on the SUNY X3B1 beamline at the National Synchrotron Light Source, Brookhaven National Laboratory. X-rays of wavelength 0.73335(2) Å were selected by a double Si(111) monochromator, and the diffracted X-rays were then selected by a Ge(111) analyzer crystal, detected by a commercial NaI scintillation detector, and then normalized to the incident beam intensity measured as a signal from an ionization chamber between the monochromator and the sample. Data were taken for 3−8 s at each 2θ step of 0.002°, with increasing counting time per step as 2θ increases. The extremely small step size of 0.002° was necessary as the sample showed a Bragg full-width-at-half-maximum of 0.02°over most of the measured angular range. Nevertheless, this is still significantly broader than the resolution of the spectrometer.

The powder pattern was indexed[17] to an orthorhombic unit cell (Table 1) with no minority phases being present. The observed systematic absences indicated either space group *Pnn*2 (No. 34) or *Pnnm* (No. 58). The number of formula units per unit cell (Z = 2) was initially estimated from the specific weight of the sample. This suggested that the Co atom was located on the site with the highest symmetry, and it was chosen as the origin in both space groups under consideration. Candidate positions for the light atoms were then found in Patterson maps.[18] Initially this was done in space group *Pnnm*; however, allowing for the (lower) *Pnn*2 symmetry made the refinement unstable and did not improve the fit. The final refinement was performed using FULLPROF.[19a] Significant anisotropic strain-broadening of the Bragg peaks was taken into account[19b] in order to achieve an acceptable fit.

(15) Bachmann, R.; DiSalvo, F. J., Jr.; Geballe, T. H.; Greene, R. L.; Howard, R. E.; King, C. N.; Kirsch, H. C.; Lee, K. N.; Schwall, R. E.; Thomas, H.-U.; Zubeck, R. B. *Rev. Sci. Instrum.* **1972**, *43*, 205.

(16) Hwang, J. S.; Lin, K. J.; Tien, C. *Rev. Sci. Instrum.* **1997**, *68*, 94.

(17) Werner, P.-E.; Eriksson, L.; Westdahl, M. *J. Appl. Crystallogr.* **1985**, *18*, 367.

(18) The structure of Fe[N(CN)$_2$]$_2$(MeOH)$_2$ was useful in visualizing the atomic bonds prior to Rietveld refinement (Manson, J. L.; Arif, A. M.; Miller, J. S. Unpublished results).

The assignment of estimated standard deviations (esds) of atomic parameters obtained from Rietveld refinements is a delicate matter. In general, the esds calculated by the Rietveld program are measures of the precision (statistical variation between equivalent experiments) rather than the accuracy (discrepancy from the correct value) of any given parameter, since the Rietveld program incorrectly considers each profile point an independent observation. We have applied an appropriate correction[20] based on the number of (a) profile points in the data set, N (i.e., 24 000), (b) independently observed peak intensities, B (i.e., 230), (c) profile parameters, P (i.e., 14), and (d) atomic parameters, C (i.e., 15).

The refined cell parameters and space group were used as input to determine the structure from powder neutron diffraction. Furthermore, when single crystals of $[Co[N(CN)_2]_2$ became available, the single-crystal structure was determined, and the details of it are reported herein.

Powder Neutron Structure Determinations. Neutron powder diffraction measurements on **2a** and **3** were made with the 32-detector BT-1 high-resolution powder diffractometer at the NIST Center for Neutron Research using a neutron wavelength of 1.5401 Å produced by a copper (311) monochromator. Collimators with horizontal divergences of 15′, 20′, and 7′ full width at half-maximum were used for the in-pile, monochromatic, and diffracted beams, respectively. The intensities were measured in steps of 0.05 in the 2θ range 3°−165° at room temperature. Each sample was powder weighing ∼4.5 g, which was loaded into a vanadium tube and positioned in the center of the beam. Neutron scattering amplitudes of 0.253, 1.03, 0.665, and 0.93×10^{-12} cm were employed for Co, Ni, C, and N, respectively. Crystal structure refinements were carried out using the program GSAS,[21] adopting as initial model the structure derived from the powder X-ray measurements described above. The space group and lattice parameters are summarized in Table 1.

The unusual broadening of some Bragg peaks, as also observed in the synchrotron X-ray experiment, suggests that anisotropic lattice strain may be present in the structure. A calculation refining the anisotropic strain-broadened peak shape parameters results in a significant improvement in the overall fit. The same model was successfully used for the structure refinement of compound **3**, which is isostructural with **2a**. An analysis of the peak shapes and splittings, however, suggests that strain broadening may not provide a complete understanding of the structural distortions, and further work will be reported elsewhere.

Single-Crystal X-ray Structure Determinations. Single crystals of **2a** were grown by slow evaporation from aqueous solution. Crystal, data collection, and refinement parameters are given in Table 1. A suitable crystal for single-crystal X-ray diffraction was selected and mounted with epoxy cement on the tip of a fine glass fiber. The data were collected on a Siemens P4 diffractometer equipped with a SMART/CCD detector. The systematic absences in the diffraction data are consistent with the space groups *Pnnm* and *Pnn*2. The *E*-statistics, the presence of a molecular 2-fold axis and mirror plane, and the value of *Z* suggested the centrosymmetric space group which yielded chemically reasonable and computationally stable results of refinement. The structure was solved by direct methods, completed by subsequent difference Fourier syntheses, and refined by full-matrix least-squares procedures. No absorption corrections were required because there was less than a 10% variation in the integrated ψ-scans intensity data. All atoms were refined with anisotropic displacement parameters. All software and sources of the scattering factors are contained in the SHELXTL (5.03) program library (G. Sheldrick, Siemens XRD, Madison, WI).

(19) (a) Rodriguez-Carvajal, J. FULLPROF Version 3.5, Dec., 1, 1997, ILL (unpublished). (b) Rodriguez-Carvajal, J.; Fernandez-Diaz, M. T.; Martinez, J. L. *J. Phys.: Condens. Mat.* **1991**, *3*, 3215.

(20) Scott, H. G. *J. Appl. Crystallogr.* **1983**, *16*, 159.

(21) Larson, A. C.; Von Dreele, R. B. *General Structure Analysis System*; Report No. LAUR-86-748, Los Alamos National Laboratory, Los Alamos, NM 87545, 1990

Table 2. Fractional Coordinates for $Ni^{II}[N(CN)_2]_2$ and $Co^{II}[N(CN)_2]_2$

	Ni	C1	N1	N2
x	0.0000	−0.2616(5)	−0.20485(29)	−0.3336(4)
y	0.0000	0.15437(34)	0.09835(24)	0.2310(4)
z	0.0000	0.34680(26)	0.20480(17)	0.5000
	Co	C1	N1	N2
x, X-ray[a]	0.0000	−0.2636(2)	−0.2082(2)	−0.3367(3)
x, neutron	0.0000	−0.2620(3)	−0.2065(2)	−0.3324(3)
y, X-ray[a]	0.0000	0.1527(2)	0.0963(2)	0.2276(3)
y, neutron	0.0000	0.1547(2)	0.0985(1)	0.2304(2)
z, X-ray[a]	0.0000	0.3478(2)	0.2085(2)	0.5000
z, neutron	0.0000	0.3480(2)	0.2083(1)	0.5000
U(eq), X-ray[a]	12(1)	16(1)	20(1)	18(1)

[a] Single-crystal data.

Table 3. Bond Distances, Å, and Angles, deg, for α-$[Co^{II}[N(CN)_2]_2$ (2a)

	295 K, neutron[a]	295 K, X-ray[a]	198 K, X-ray[b]
	Bond Distance, Å		
Co−N1	2.095(1)	2.09(1)	2.1008(14)
Co−N2	2.162(2)	2.17(1)	2.161(2)
C1−N1	1.156(1)	1.14(2)	1.156(2)
C1−N2	1.315(1)	1.33(1)	1.321(2)
Co···Co	5.930,[c] 5.985, 7.103, 7.394	5.933,[c] 6.011, 7.072, 7.393	5.936,[c] 5.998, 7.071, 7.417
	Bond Angle, deg		
N1−Co−N1	85.36(5), 94.64(5), 180.00	85.2(4), 94.8(4), 180.00	85.24(8), 94.76(8), 180.00
N1−C1−N2	175.34(18)	176(1)	175.3(2)
Co−N1−C1	160.34(12)	160.6(8)	160.08(12)
C1−N2−C1	117.43(20)	118.1(8)	120.3(2)

[a] Powder. [b] Single crystal. [c] CoNCNCNCo.

Table 4. Average Bond Distances, Å, and Angles, deg, for $Ni^{II}[N(CN)_2]_2$ (3)

bond distances		bond angles	
Ni−N1	2.0512(14)	N1−Ni−N1	86.51(9), 93.49(9), 180.0
Ni−N2	2.1369(24)	N1−C1−N2	174.87(28)
C1−N1	1.1588(24)	Ni−N1−C1	160.06(19)
C1−N2	1.3131(22)	C1−N2−C1	116.65(31)
Ni···Ni	5.881,[a] 5.974, 7.032, 7.294		

[a] NiNCNCNNi.

Results and Discussion

Crystal Structure. The structural analyses show that **2a** and **3** are isomorphous, crystallize in the orthorhombic space group *Pnnm* with two molecules per unit cell (Tables 1−4), and are isomorphous to $Cu^{II}[N(CN)_2]_2$.[14a] The M^{II} ions for **2a** and **3** sit on an inversion center and N2 (Figure 1) resides on a mirror plane perpendicular to the *c*-axis. Rietveld analyses of the powder neutron and X-ray diffraction data were determined at 295 K for **2a** and **3**, while the single-crystal X-ray structure was determined at 195 K (−78 °C). The M is six-coordinate and bound to six different μ_3-bonded $[N(CN)_2]^-$ ligands, **1b** (Figure 1), forming a noninterpenetrating 3-D framework (Figures 2a and 3) akin to rutile (TiO_2) (Figure 2b). Each octahedral M^{II} site is slightly tetragonally elongated with average axial M−N distances of 2.161(5) (**2a**) and 2.137(2) (**3**) Å and average equatorial Mn−N distances of 2.091(4) (**2a**) and 2.051(1) (**3**) at room temperature. This is in contrast to rutile-type $M^{II}[C(CN)_3]_2$ (M = V, Cr, Mn, Fe, Co, Ni,

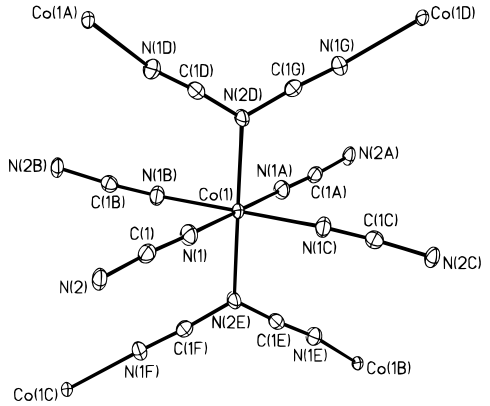

Figure 1. Atom labeling diagram and ORTEP (30% probability level) diagram for α-[$Co^{II}[N(CN)_2]_2$, **2a**, obtained by single-crystal X-ray diffraction. The axial M−N distances are 2.161(5) (**2a**) and 2.137(2) (**3**) Å and equatorial M−N distances of 2.091(4) (**2a**) and 2.051(1) (**3**) Å. Note the axial ligands are $N(CN)_2$ bound, while the equatorial ligands are terminally bound, i.e., −NCNCN−.

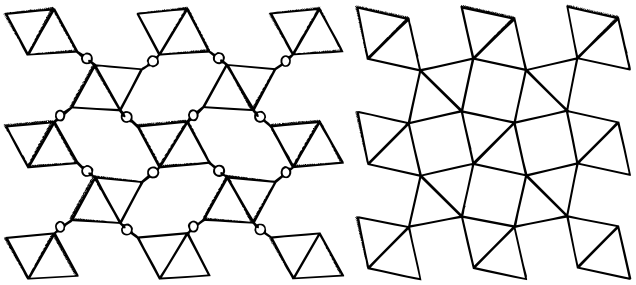

Figure 2. Polyhedral framework structure of $M^{II}[N(CN)_2]_2$ (left) and rutile (TiO_2) (right).

Cu), which has cavities of sufficient size to allow interpenetration of a second identical lattice.[11b,c] Each M^{II} is coordinated to four equatorial $[N(CN)_2]^-$ ligands that bridge between two adjacent Co^{II} sites, generating ribbon-like 1-D chains that propagate along the *c*-axis (Figure 3). Adjacent parallel chains pass through the center of the unit cell and pack out-of-registry with the central N2s bridging to M^{II} ions of adjacent chains to form a 3-D network. $[N(CN)_2]^-$ has pseudo-C_{2v} symmetry with average C1≡N1 distances of 1.158 (**2a**) and 1.159 Å (**3**), at room temperature and C1−N2 distances of 1.315 (**2a**) and 1.313 (**3**) Å. These values are similar to that observed in other materials.[12] Due to crystal packing forces the N2−C1≡N1 bond angles deviate slightly from linearity and average 175.3 (**2a**) and 174.9° (**3**) for M = Co and Ni, respectively. Each M^{II} site is slightly distorted from O_h symmetry with average M−N1 and M−N2 distances of 2.096 and 2.170 (**2a**) and 2.051 and 2.137 (**3**) Å, respectively, and with cis N−Co−N′ bond angles ranging from 85.21° and 94.79°. Furthermore, the shortest M···M separations of 5.936 (**2a**) and 5.881 (**3**) Å are substantially shorter than the 7.679 Å observed for $Mn^{II}[C(CN)_3]_2$.[11b,22]

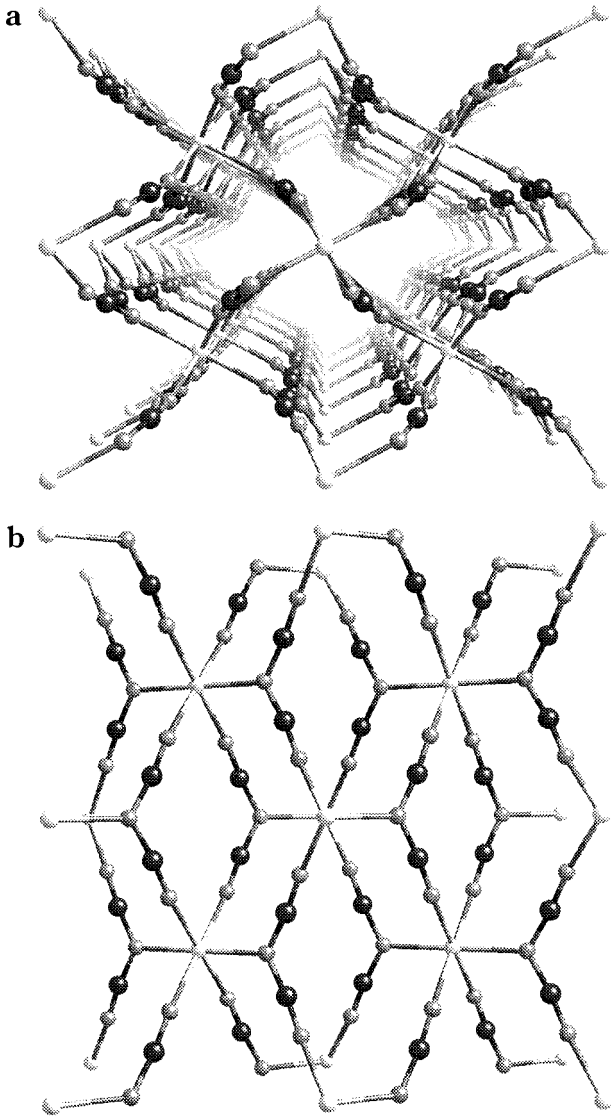

Figure 3. Perspective view down the *c* (a) and *a* axes (b) of $Co^{II}[N(CN)_2]_2$ (**2a**) (**3** is isomorphous).

The structure of **2b** has yet to be elucidated due to poor diffraction; however, on the basis of the optical and magnetic properties (vide infra), the Co^{II} is assigned to be tetrahedral, as observed for $Zn[N(CN)_2]_2$,[23] in contrast to **2a**. On the basis of this tetrahedral geometry and stoichiometry, $[N(CN)_2]_2^-$ is assumed to bridge in a trans-μ fashion, i.e., **1b** or **1c**. For the more symmetrical **1b** linkage, a variety of motifs, including 2-D layered, e.g., **4**, and 3-D diamondlike structures, are possible. For the asymmetrical **1c** linkage as well as well as combinations of the **1b** or **1c** linkages, more complex, including interpenetrating, structures are envisioned.

Electronic Structure. Solid-state reflectance spectra were obtained in the UV−visible region for **2a**, **2b**, and **3** and are shown collectively in Figure 4. Compound **2a** exhibits two closely spaced bands at 19 700 and 20 900 cm^{-1} assigned to the $^4T_{1g}(F) \rightarrow {}^4A_{2g}(F)$ and $^4T_{1g}(F) \rightarrow {}^4T_{1g}(P)$ transitions, respectively, in agreement with the octahedral symmetry. In comparison, the

(22) Note for comparison purposes we report the distances obtained from powder neutron diffraction at 295 K. The powder synchrotron refinement yielded similar results utilizing anisotropic strain-broadening of the Bragg peaks. Powder neutron diffraction data were initially refined to give two very slightly different phases with the phases having $a = 5.97369$ (29) Å, $b = 7.11869$ (32) Å, $c = 7.39532$ (20) Å, and $a = 6.00735$ (34) Å, $b = 7.08364$ (37) Å, $c = 7.3953$ (20) Å. Use of anisotropic strain-broadening of the Bragg peaks enabled the refinement of only one phase presented herein.

(23) Manson, J. L.; Lee, D. W.; Rheingold, A. L.; Miller, J. S. Submitted.

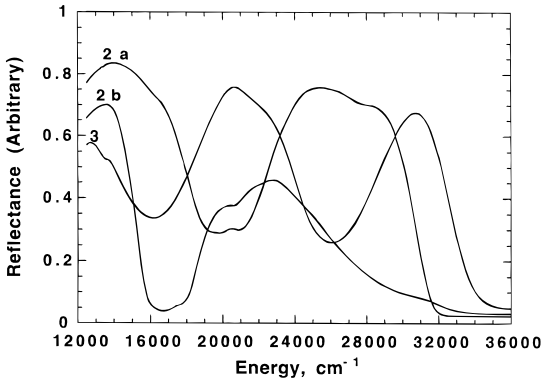

Figure 4. Solid-state UV−visible reflectance spectra of **2a**, **2b**, and **3**.

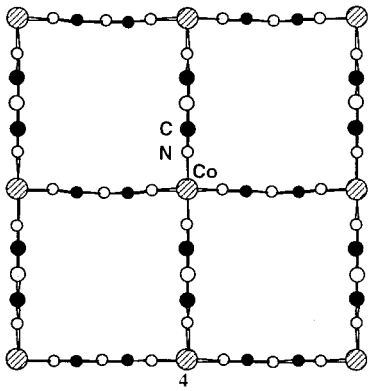

electronic spectra of $[Co(OH_2)_6]^{2+}$ shows bands at 19 600 and 21 600 cm^{-1}, while $[Co(NCMe)_6]^{2+}$ features two transitions of slightly higher energy at 20 300 and 21 200 cm^{-1}, respectively, suggesting comparable ligand-field strengths.[24a] In the spectrochemical series, acetonitrile is similar to ammonia, but is a slightly stronger field ligand than water.[25] Hence, dicyanamide is expected to be a weak-field ligand equivalent to acetonitrile, as noted. Tetrahedral Co^{II} compounds such as $[CoCl_4]^{2-}$ display a weak band of low energy at 5800 cm^{-1} and a more intense band higher in energy at 15 000 cm^{-1} and are assigned to $^4A_2(F) \rightarrow {}^4T_1(F)$ and $^4A_2(F) \rightarrow {}^4T_1(P)$, respectively.[24a] Since the near-IR region was experimentally inaccessible, **2b** shows only a single band at 16 800 cm^{-1}, significantly higher in energy than that found for $[CoCl_4]^{2-}$. This is expected due to the much weaker ligand field imposed by the polarizable Cl^- ligand, in contrast to stronger field nitrile-type ligands. Octahedral Ni^{II} typically exhibits two bands near 15 500 and 25 500 cm^{-1}, attributed to $^3A_{2g}(F) \rightarrow {}^3T_{1g}(F)$ and $^3A_{2g}(F) \rightarrow {}^3T_{1g}(P)$ transitions, respectively, and consistent with the spectra of **3**, which shows bands of comparable energy at 16 100 and 26 000 cm^{-1}.[24b]

Magnetic Properties. The temperature dependence of the magnetic susceptibility, χ, can be fit by the Curie−Weiss expression, $\chi(T-\theta)^{-1}$, as shown in Figure 5, with $g = 2.60$, $\theta = 9$ K ($T > 50$ K); $g = 2.27$, $\theta = -7$ K ($T >$

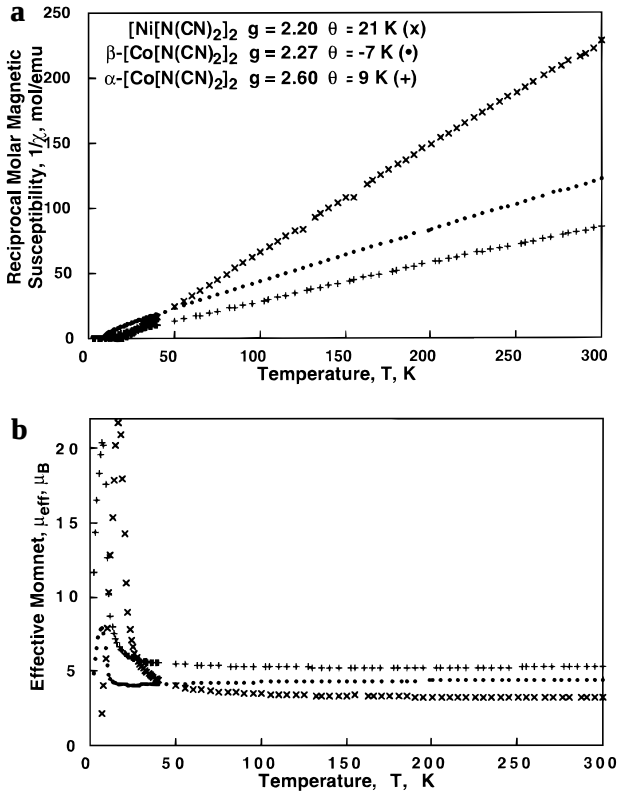

Figure 5. Reciprocal molar magnetic susceptibility, χ^{-1} (a), and moment, μ_{eff} (b), as a function of temperature (1000 Oe) for $M^{II}[N(CN)_2]_2$ [M = α-Co (+) (**2a**), β-Co (●) (**2b**), and Ni (×) (**3**)].

60 K); and $g = 2.20$, $\theta = 21$ K ($T > 50$ K) for **2a**, **2b**, and **3**, respectively, indicative of ferromagnetic coupling between the M^{II} metal centers for **2a** and **3** and antiferromagnetic coupling for **2b**. The θ-values for **2a** and **3** are consistent with the recently obtained values for these compounds.[14a] These g values are as expected for octahedral Co^{II}, tetrahedral Co^{II}, and octahedral Ni^{II}, respectively.[26a] It is interesting to note that the θ-value of **2b** is of the same magnitude as found in **2a**, suggesting interactions of similar strength, but of opposite sign. At 300 K, the effective moments, μ_{eff} [$\equiv(8\chi T)^{1/2}$] are 5.13 (**2a**), 4.36 (**2b**), and 3.17 μ_B (**3**) (Figure 5) in accord with their expected g-values.[26a] As is typical for Co^{II} and Ni^{II}, these values are significantly higher than their respective spin-only values due to spin−orbit coupling and are comparable to values observed in many other related systems[23,27] and in particular are comparable to the 4.98 (**2a**), 4.60 (**2b**), and 3.18 μ_B (**3**) reported earlier.[13] The effective moment for **2a** remains nearly constant at 5.13 μ_B from 300 K down to ~100 K, followed by a rapid increase to a maximum value of 21 μ_B in an applied magnetic field, H_{dc}, of 1 kOe at 7 K, due to ferromagnetic coupling. μ_{eff} decreases abruptly below 7 K due to slowly increasing magnetization below T_c and decreases further to 2 K. Similar behavior is observed for **3**, except

(24) (a) Figgis, B. N. *Introduction to Ligand Fields*; Interscience: New York, 1966; Chapter 9. Ballhausen, C. J. *Introduction to Ligand Field Theory*; McGraw-Hill: New York, pp 255−259. (b) Drago, R. S. *Physical Methods for Chemists*, 2nd ed.; Saunders: New York, 1992; Chapter 10. Lever, A. B. P. *Inorganic Electronic Spectroscopy*, 2nd ed.; Elsevier: New York, 1984.

(25) Buschmann, W. E.; Miller, J. S. *Chem. Eur. J.* **1998**, *4*, 17341.

(26) (a) Carlin, R. L. *Magnetochemistry*; Spinger-Verlag: New York, 1986; pp 65−68. (b) *ibid*. p121. (c) Robinson, W. K.; Friedberg, S. A. *Phys. Rev.* **1960**, *117*, 402.

(27) (a) Figgis, B. N. In *Comprehensive Coordination Chemistry*; Wilkinson, G., Ed.; Pergamon: New York, 1987, *1*, 271−274. (b) Hathaway, B. J.; Holah, D. G. *J. Chem. Soc.* **1964**, 2400. (c) Hathaway, B. J.; Holah, D. G.; Underhill, A. E. *J. Chem. Soc.* **1962**, 2444. (d) Hathaway, B. J.; Holah, D. G. *J. Chem. Soc.* **1964**, 2408. (e) Fackler, J. P.; Holah, D. G. *Inorg. Chem.* **1965**, *4*, 954.

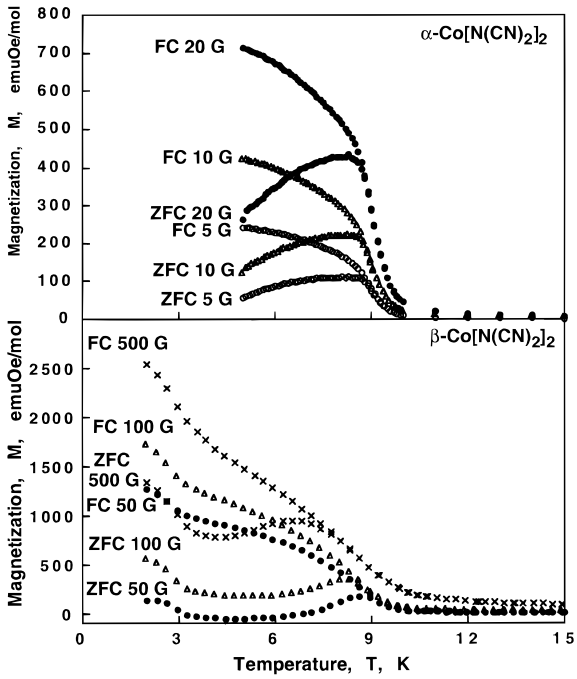

Figure 6. Field-cooled and zero-field-cooled M(T) data for α-(**2a**) and β-$Co^{II}[N(CN)_2]_2$ (**2b**).

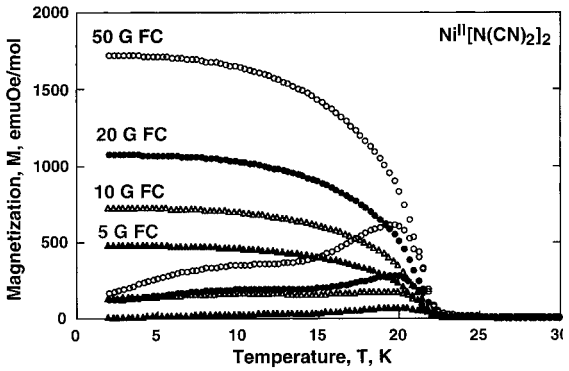

Figure 7. Field-cooled and zero-field-cooled M(T) data for $Ni^{II}[N(CN)_2]_2$ (**3**).

a maximum value of 23 μ_B (H_{dc} = 1 kOe) is observed at 17 K before falling off quickly down to 2 K. In contrast, the effective moment for **2b** decreases gradually as the temperature is reduced from 300 to 50 K and reaches a minimum at 28 K before rapidly increasing to a maximum of 7.2 μ_B at 6.9 K (H_{dc} = 1 kOe), suggesting the onset of ordered magnetic behavior. Finally, a sharp decrease upon cooling to 2 K due to magnetic ordering or saturation is also observed.

The low-field field-cooled (FC) and zero-field-cooled (ZFC) temperature dependence of the magnetization acquired while warming from the lowest temperature reveals magnetic ordering below essentially magnetic field independent bifurcation temperatures, T_b, of 9.2 (**2a**) and 20.6 K (**3**) at all fields measured (Figures 6 and 7). For **2b**, a markedly different behavior occurs. The data taken at 50 and 100 G show very similar behavior with the T_b shifting from 9.2 (50 G) to 8.5 K (100 G). At 500 G, bifurcation shifts to even lower temperature (8.0 K) with a significantly broader maximum but then shows features similar to those measured at smaller H. The field dependence of the bifurcation temperature suggests glassiness in **2b**.

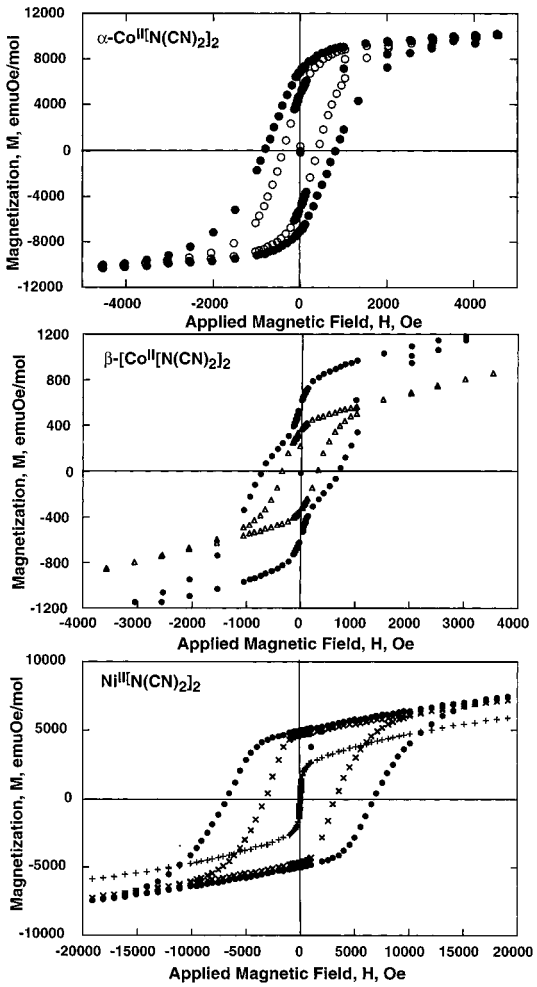

Figure 8. Hysteresis loops, $M(H)$, α-$Co^{II}[N(CN)_2]_2$ (**2a**) at 2 K (●, H_c = 800 Oe) and 5 K (o; H_c = 425 Oe), top, β-$Co^{II}[N(CN)_2]_2$ (**2b**) at 2 K (●, H_c = 680 Oe) and 6 K (Δ; H_c = 330 Oe) (middle), and $Ni^{II}[N(CN)_2]_2$ (**3**) at 2 K (●, H_c = 7,000 Oe), 11 K (×), and 20 K (+) (bottom).

The ferromagnetic behavior for **2a** and **3** is supported by the 5 K, 5.5 T saturation magnetization, M_s, values from 14 000 (**2a**) to 11 900 emu Oe/mol (**3**). **2b** initially shows a rapid rise of its 5 K magnetization to ~3000 emu Oe/mol at 0.3 T. Its magnetization then increases with a linear slope to 3 T and then begins to show some curvature approaching 11 400 emu Oe/mol at 5 T. The 2 K M_s for **3** is close to that predicted using the g-values obtained from the Curie−Weiss fit (12 300 emu Oe/mol) with the deviation attributed to having not yet achieved saturation at the largest measuring field. In contrast, the 5 K M_s for **2a** and **2b** are much lower than that predicted by using the g-values obtained from the Curie−Weiss fit [21 800 (**2a**) and 19 000 (**2b**) emu Oe/mol]. This deviation for **2a** is attributed to the effects of Kramers doublet formation at low-temperature, giving an effective spin of $^1/_2$ with g = 5.03, as determined form the 5 K $M(H)$ data. This is comparable to other octahedral Co^{II} compounds.[26c] The rapid rise and approach to saturation in the $M(H)$ data at low temperatures for both **2a** and **3** (Figure 8) is typical for long-range ferromagnetic coupling. Hysteresis loops characteristic of ferromagnetic behavior with coercive fields, H_{cr}, of 800 (**2a**) and 7000 Oe (**3**) were observed at 2 K (Figure 8). The 7000 Oe value for **3** is substantially

greater than the 191 Oe value recently reported (although the temperature at which these data was taken was not noted).[14a]

Hysteretic behavior was also observed for **2b** at 2 and 6 K (Figure 8). At 2 K, **2b** has a coercive field, H_{cr}, of 680 Oe, although at the highest field measured, 5 T, the magnetization reaches a value of 4650 emu Oe/mol and saturation is not achieved. This value lies slightly below the 5585 emu Oe/mol expected for a $S = {}^1/_2$, $g = 2$ system. The shape of the 2 K hysteresis loop is constricted, in contrast to ferromagnets or antiferromagnets, and suggests the presence of a spin-canted state. For tetrahedral Co^{II} metal centers, a $^4A_2$ ground state is predicted and at low temperatures an effective spin of $^1/_2$ results.[26] Furthermore, zero-field splitting can be rather large, and in fact, a value of 14 K ($H = -2J\mathbf{S}_a\cdot\mathbf{S}_b$) is observed in Cs_2CoCl_4.[28] At 6 K, a somewhat reduced H_{cr} of 330 Oe is observed. The magnetization is 3825 emu Oe/mol at 5 T, although saturation does not occur. The $M(H)$ behavior from about 1 to 5 T at 2 and 6 K possesses characteristics akin to a simple antiferromagnet, i.e. a nearly linear $M(H)$ response to the applied magnetic field.

To confirm the magnetic ordering, the temperature dependencies of the in-phase, $\chi'(T)$, real, and out-of-phase, $\chi''(T)$, imaginary, components of the complex ac susceptibility were measured. A peak in 10 Hz $\chi'(T)$, $T_{\chi'}$, is attributed to bulk magnetic ordering and is observed at 8.7 and 19.7 K for **2a** and **3**, respectively (Figure 9) in accord with recent work.[14a] This is in excellent agreement with the $M(T)$ bifurcation data (Figures 6 and 7). Ferromagnetic coupling is evident due to the existence of a nonzero $\chi''(T)$ (out-of-phase) component.[29a]

A measure of glassiness of a material can be determined from the frequency dependence, f, of the temperature at which the $\chi'_{ac}(T,f)$ has a maximum for data taken between 10 and 1000 Hz via eq 1.[29b]

$$\phi = \frac{T^{ac}_{max}(10\text{Hz}) - T^{ac}_{max}(1000\text{ Hz})}{2T^{ac}_{max}(10\text{ Hz})} \qquad (1)$$

The modest values of ϕ, i.e., 0.003 (**2a**), 0.002 (**2b**, T_{c1}), 0.007 (**2b**, T_{c2}), and 0.002 (**3**), suggest the presence of aspects of spin-glass behavior for these ordered compounds. By comparison, values of zero, as observed for $[MnOEP][C_4(CN)_6]$,[30] indicate no glassiness, while a value of 0.28 is observed for the superparamagnet α-$Ho_2O_3\cdot B_2O_3$.[29b]

The presence of two peaks in χ''(T) indicates irreversibility, as expected for canted magnets. The high-temperature peak is of much larger magnitude than the low-temperature peak. This suggests the possibility of two independent canting transitions in the same material, of which similar behavior has been observed in other molecule-based magnets such as $[MnOEP][C_4(CN)_6]$.[30] To identify the nature of the spin canting,

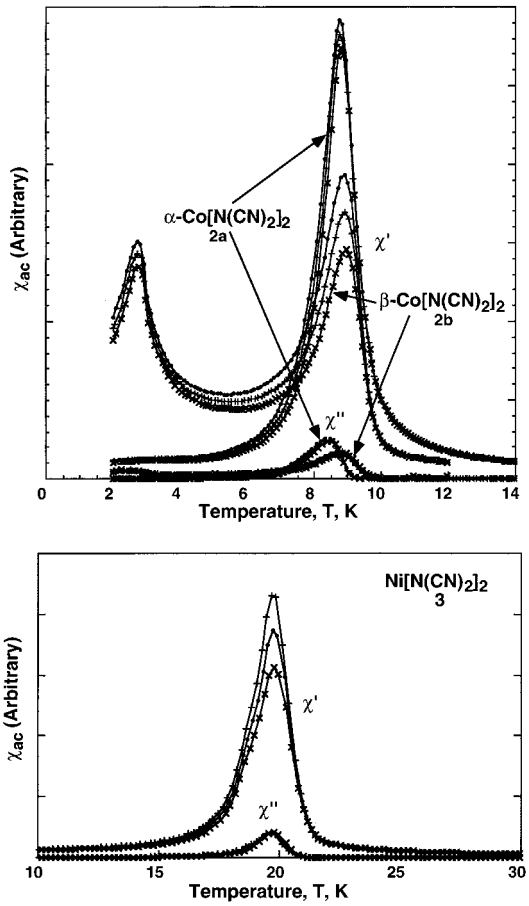

Figure 9. Dispersive, χ' (●, ▲, and ▼), and absorptive, χ'' (●, ▲, and ▼), components of the ac susceptibility at 10, 10^2, and 10^3 Hz, respectively, for $M^{II}[N(CN)_2]_2$ [M = α- (**2a**) and β-Co (**2b**), Ni (**3**)]. (H_{dc} = 0 Oe, amplitude = 1 Oe). Samples were zero-field-cooled and data taken upon warming.

additional measurements such as neutron diffraction are required and are in progress. Note that the high-temperature transition in **2b** may be due to a residual amount of **2a**.

The close agreement between the θ values and the T_cs supports a three-dimensional magnetic phase transition. Using θ values of 9 (**2a**), −7 (**2b**), and 21 K (**3**) and the mean field result, i.e., $J/k_B = 3\theta/[2zS(S+1)]$,[26b] yields values for J/k_B of 0.45, −0.7, and 2.0 K for **2a**, **2b** and **3**, respectively, assuming the number of nearest neighbors, z, is 8 for **2a** and **3**, and 4 for **2b**. Preliminary temperature-dependent specific heat studies have peaks at 9.4 (**2a**), 2.4 and 8.4 (**2b**), and 21.1 K (**3**), consistent with the T_c obtained from the $\chi'(T, 10\text{ Hz})$ data.

Conclusion

Dicyanamide forms a series of homoleptic 2:1 complexes with first-row divalent metal ions. The metal can either be four (**2b**) or six (**2a**, **3**) coordinate. Magnetic ordering is observed for the three examples reported herein (Table 5).[31] Ferromagnetic ordering at 9.4 and 21.1 K is observed for the octahedral Co (**2a**) and Ni (**3**)

(28) (a) Carlin, R. L. *J. Appl. Phys.* **1981**, *52*, 1993. (b) Carlin, R. L. *Science* **1985**, *227*, 1291.

(29) (a) Mukherjee, S.; Ranganathan, R.; Roy, S. B. *Phys. Rev. B* **1994**, *50*, 1084. (b) Mydosh, J. A. *Spin glasses: an Experimental Introduction*; Taylor & Francis: London, Washington, D. C., 1993; p 66.

(30) Wynn, C. M.; M. Gîrtu, M.; Miller, J. S.; Epstein, A. J. *Phys. Rev. B* **1997**, *56*, 14050.

(31) Antiferromagnetic ordering is observed for the phase of $Mn^{II}[N(CN)_2]_2$ isomorphous to **2a** and **3** (Manson, J. L.; Kmety, C. R.; Huang, Q−z.; Lynn, J. W.; Bendele, G. M.; Pagola, S.; Stephens, P. W.; Epstein, A. J.; Miller, J. S. Manuscript in preparation).

Table 5. Summary of the Magnetic Properties of $M^{II}[N(CN)_2]_2$ (M = Co, Ni)

	α-Co[N(CN)$_2$]$_2$, **2a**	β-Co[N(CN)$_2$]$_2$, **2b**	Ni[N(CN)$_2$]$_2$, **3**
no. of nearest neighbors, z	8	4	8
θ, K (high T)	9[a]	−7	21[b]
g (high T)	2.60	2.27	2.20
μ_{eff} (300 K), μ_B	5.13	4.36	3.17
M, emu Oe/mol (5 K, 5.5 T)	14000	4650	11900
H_c, Oe (2 K)	800	680	7000[c]
T_b, bifurcation temp, K	9.2	9.2	20.6
T_c, $T_{\chi'}$ [maxima in χ'(T, 10 Hz)], K	8.7	2.7, 8.9	19.7
maximum in $c_p(T)$	9.4	2.4, 8.4	21.1
$J(z)$, K/k_B (mean field)	0.45	−0.7	2.0

[a] 6.1 K. [b] 21.4 K.[14a] [c] 191 Oe (T unknown).[14a]

compounds, respectively, while the tetrahedral Co compound (**2b**) exhibits two transitions states at 2.59 and 8.35 K preliminary assigned to be canted states. The coercive fields range from 680 (**2b**) to 7000 Oe (**3**), and unexpectedly, the coercivity for the Ni (**3**) compound is substantial greater than that of the isomorphous Co (**2a**) compound. The magnetic ordering for octahedral **2a** and **3** is in sharp contrast to the absence of magnetic ordering for interpenetrating rutile structures M[C(CN)$_3$]$_2$ (M = Co, Ni). This is attributed to strong ferromagnetic coupling via the three-atom M−N(CN)$_2$ bond, which is not present for M[C(CN)$_3$]$_2$.[11b,c]

Acknowledgment. The authors gratefully acknowledge the support from the U. S. Department of Energy (DOE) Division of Basic Energy Sciences (Grant Nos. DE-FG02-86ER45271 and DE-FG03-93ER45504), the Division of Advanced Materials (DE-FG02-96ER12198), and the U.S. National Science Foundation (NSF) (Grant No. DMR95-01325). The SUNY X3 beamline at the National Synchrotron Light Source is supported by the Division of Basic Energy Sciences (DE-FG02-86ER45231). Research carried out at the NSLS at Brookhaven National Laboratory is supported by the DOE, Division of Materials Sciences and Division of Chemical Sciences. L.L-S. and A.L.R. acknowledge the NSF (CHE-9628768) for their support in the purchase of the diffractometer. We thank Dr. M. Kurmoo for discussing his unpublished work and sharing of a preprint disclosing the structure and magnetic properties of Cu[N(CN)$_2$]$_2$, as well as R. Black and J. Diederichs (Quantum Design, San Diego, CA) for acquiring the specific heat data, R. Dinnebier for useful contributions to preliminary phases of the synchrotron X-ray studies, and S. Shield (University of Utah) for aid in obtaining the optical data.

Supporting Information Available: A summary of the crystallographic data, tables of fractional coordinates and anisotropic thermal parameters, indices and integrated intensities of the strongest lines in the X-ray powder diffraction pattern, as well as bond distances and angles for **2a** and **3** (11 pages); calculated and observed structure factors for **2a** (1 page). Ordering information is given on any current masthead page.

CM980321Y